Clustering of Salt Fingers in Double-Diffusive Convection Leads to Staircaselike Stratification

Francesco Paparella[1] and Jost von Hardenberg[2]
[1]Dipartimento di Matematica e Fisica "Ennio De Giorgi," Università del Salento, 73100 Lecce, Italy
[2]ISAC-CNR, Corso Fiume 4, 10133 Torino, Italy
(Received 29 March 2012; published 6 July 2012)

We report on high-resolution, three-dimensional, high Rayleigh number, and low density ratio numerical simulations of fingering convection. We observe a previously unreported phenomenon of self-organization of fingers that cluster together to form larger-scale coherent structures. The flow ultimately forms density staircases, alternating well-mixed regions with fingering convective zones. We give evidence that the mechanical mixing induced by the clusters forms the staircases with a mechanism analogous to staircase formation in a stably stratified, nonconvective, stirred fluid.

DOI: 10.1103/PhysRevLett.109.014502 PACS numbers: 47.20.Bp, 47.55.P−, 92.10.af

Fingering convection plays an important role in many fields, ranging from stellar astrophysics to metallurgy [1], and is of particular interest in oceanography, where it may generate large heat and salt fluxes with an impact on the global circulation and on climate [2–4]. This peculiar convective flow occurs when two buoyancy-changing scalars with different diffusivities, such as salt and temperature, make an overall bottom-heavy density stratification, but the least-diffusing one, taken alone, would produce a top-heavy stratification. In the fingering regime, a fluid parcel displaced from its equilibrium height exchanges the better diffusing and stabilizing scalar faster than it exchanges the destabilizing one, developing a buoyancy anomaly that further increases the displacement. The linear stability properties of the doubly diffusive instability are well understood [3,5,6] and, close to marginality, tall, fingerlike convection plumes emerge (hence the name). Far from the instability, in the highly nonlinear regime, these tall structures appear just as a short transient, after which the convection is sustained by the motion of almost spherical, bloblike structures [3,7], and the statistics of the fluctuations of the scalars become non-Gaussian [8].

An intriguing phenomenon that happens at high Rayleigh number and low density ratio (a measure of the relative contribution to the buoyancy of the two scalars) is an instability of the horizontally averaged profiles of temperature, salinity, and buoyancy. Laboratory experiments show that initially constant vertical gradients develop kinks which steepen and evolve into an alternation of well-mixed zones characterized by Bénard-like convection cells and high-gradient layers populated by fingers [9]. Such staircase profiles are found in the main thermocline of the subtropical oceans and of many marginal seas [2]. The staircase-forming regime of fingering convection has eluded numerical simulations for a long time, so long, in fact, that doubts were cast on its reality [7]. Recently, a report on numerical simulations reproducing staircases in a vertically periodic domain has been published [10].

In this Letter, we report on three-dimensional staircase-forming simulations with temperature and salinity held fixed at rigid top and bottom plates, as in the experiments of R. Krishnamurti [9]. We work in a regime of very low density ratio and high Rayleigh number, associated with very high numerical resolution (to our knowledge unprecedented for this problem). We find a previously unreported phenomenon of self-organization of fingers that cluster together to form large-scale coherent structures. This is reminiscent of the clustering of plumes in high aspect-ratio Rayleigh-Bénard convection [11,12]. We suggest a mechanism of staircase formation that occurs in two phases: first, the fingers group to form coherent structures at larger scales; then, the mechanical mixing induced by those clusters forms the staircases with a mechanism analogous to that of staircase formation in a stably stratified (nonconvective) stirred fluid [13–18].

The nondimensional equations of motion of fingering convection, in the Boussinesq approximation, are

$$\frac{\partial \mathbf{u}}{\partial t} + \mathbf{u}\cdot\nabla\mathbf{u} = -\nabla p + \mathrm{PrLe}[R_S B\hat{\mathbf{z}} + \nabla^2\mathbf{u}], \quad (1)$$

$$\frac{\partial T}{\partial t} + \mathbf{u}\cdot\nabla T = \mathrm{Le}\nabla^2 T, \quad (2)$$

$$\frac{\partial S}{\partial t} + \mathbf{u}\cdot\nabla S = \nabla^2 S, \quad (3)$$

$$\nabla\cdot\mathbf{u} = 0, \quad (4)$$

where we have denoted the least-diffusing scalar as salinity, S, and the most-diffusing one as temperature, T. Here, $\mathbf{u} = (u, v, w)$ is the solenoidal velocity field of the fluid, p is the pressure, $\hat{\mathbf{z}}$ is the vertical unit vector, and we have defined the buoyancy field $B = R_\rho T - S$.

The problem has been brought to a nondimensional form by scaling temperature and salinity with their plate differences ΔT and ΔS, scaling lengths with the layer thickness, d, and using the haline diffusive time, $\tau_S = d^2/\kappa_S$, as a

time scale, with κ_S the haline diffusivity [8]. The nondimensional control parameters of the problem are the Prandtl number, $\mathrm{Pr} = \frac{\nu}{\kappa_T}$, the Lewis number, $\mathrm{Le} = \frac{\kappa_T}{\kappa_S}$, the haline Rayleigh number, $R_S = \frac{g\beta\Delta S d^3}{\nu\kappa_S}$, and the density ratio, $R_\rho = \frac{\alpha\Delta T}{\beta\Delta S}$. In these expressions, ν is the kinematic viscosity, κ_T is the thermal diffusivity, g is the modulus of the gravity acceleration, and α and β are the linear thermal and haline expansion coefficients. For uniform vertical gradients of the initial stratification, a necessary condition for the fingering instability to occur is $1 < R_\rho < \mathrm{Le}$ [3].

We integrate the equations numerically with a hybrid spectral-finite difference code with laterally periodic and free-slip top and bottom boundary conditions [11,19]. The initial condition is a random perturbation of the conductive solution. We fix the parameters at $R_S = 10^{13}$, $\mathrm{Pr} = 10$, $\mathrm{Le} = 3$, and $R_\rho = 1.025$. These choices represent an extremely high Rayleigh number and low density ratio, ensuring a vigorous convection. The domain is a slab of sizes $L_x = 0.2$, $L_y = 0.05$, $L_z = 1$ with corresponding resolutions $N_x = 768$, $N_y = 192$, $N_z = 5120$ grid points which adequately resolve both the steep boundary layers and the equally high gradients at the fingertips. A horizontal section of the domain contains approximately 32×8 finger widths, estimated as the half-wavelength $l_f = \pi\{\mathrm{Le}/[R_s(R_\rho - 1)]\}^{0.25} \approx 0.006$ of the fastest growing mode [3]. The simulation was continued up to nondimensional time $t = 1.5 \times 10^{-5}$, with a time step $\Delta t = 10^{-10}$, requiring a total of 150 000 core hours, using 128 cores on a parallel supercomputer [20].

After an initial transient in which the upper and lower boundary layers form, the flow is characterized by the emergence of intense bloblike structures (we shall still call them fingers) which create a vigorous up-gradient vertical buoyancy flux. Figure 1 shows vertical sections of the salinity anomaly at three different times. Already at an early stage, a large number of fingers are visible [Fig. 1(a)]. They are characterized by typical mushroom-like tips, similar to the plumes of thermal convection, and are homogenously distributed in the domain. As time evolves, we observe a completely new phenomenon, as the fingers tend to cluster together to form larger-scale structures [Figs. 1(b) and 1(c)] which ultimately reach a horizontal extension which is comparable to the size of the domain.

The growth of the characteristic scales in the flow with the generation of large-scale structures is illustrated in Fig. 2, showing kinetic energy spectra $E(k)$ as a function of the horizontal wavelength, $\lambda = 2\pi/k$, for the three times shown in Fig. 1. At the earliest time, we recognize a clear spectral peak at the wavelength of finger formation. Later, the spectra evolve as more and more kinetic energy appears at large scales, until the spectral maximum reaches the scale of the box. To characterize the evolution of the spectra, we show in the inset of Fig. 2 the growth in time of

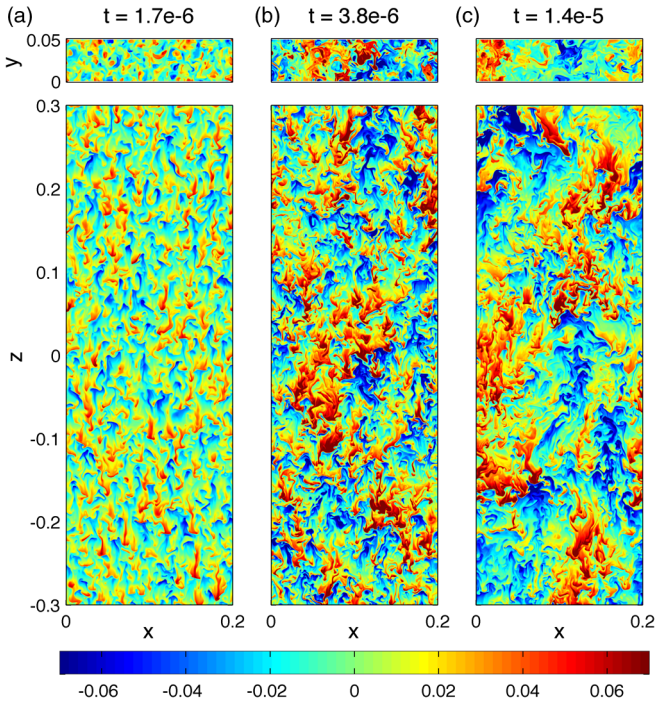

FIG. 1 (color online). Vertical sections at $y = L_y/2$ (lower panels) and horizontal sections at $z = 0$ (upper panels) of salt anomaly, $S'(x, y, z) = S(x, y, z) - \bar{S}(z)$, in the central portion of the domain $-0.3 < z < 0.3$, at three different times.

the integral scale $\Lambda = 2\pi \int [E(k)/k]dk / \int E(k)dk$, which we use to define a characteristic size of the largest dynamical flow structures [11,12]. Starting from the characteristic scale of fingers, the integral scale grows until it becomes comparable to the size of the box. A sequence of intense oscillations follows, which are correlated with oscillations

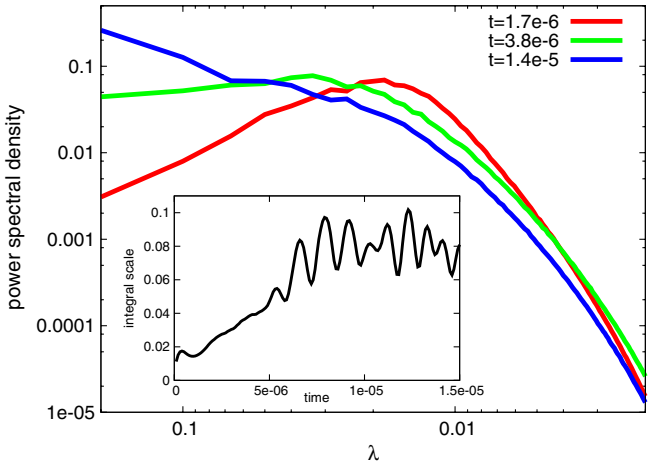

FIG. 2 (color online). Evolution with time of total kinetic energy spectra as a function of the horizontal wavelength ($\lambda = 2\pi/k$). The spectra have been averaged over the central portion of the domain (from $-0.3 < z < 0.3$) and over three consecutive time steps spaced $\delta t = 10^{-7}$. The inset shows the time evolution of the integral scale Λ defined in the text.

in the vertical convective buoyancy flux (not shown) and with a period which is comparable with the buoyancy period $\tau_{\text{buoy}} = 2\pi/\sqrt{\text{PrLe}R_S(R_\rho - 1)}$. We associate this evolution with the initial formation of finger clusters, leading to a growth of the average scales in the flow, followed by a regime in which the flow is dominated by the motion and large-scale dynamical interactions between the clusters.

The structure of the finger clusters is illustrated by enlargements of vertical sections of the flow in Fig. 3. The temperature and salinity fields confirm that individual, mushroom-tipped fingers of the same sign tend to group together. The smoother vertical velocity field shows that those clusters form a coherent whole moving together. The buoyancy field shows the fine internal structure of the clusters, where anomalies of both signs are found. However, spatial low-pass filtering of the buoyancy field (not shown) reveals the prevalence of contributions with the same sign as the cluster's vertical velocity. These figures illustrate the mechanism at work for the formation of the clusters: when a few fingers of the same sign happen to be close to each other, dragging further fluid with them, they create scalar anomalies which may trigger the double-diffusive instability and promote the formation of new fingers. In fact, earlier evidence shows that at high Rayleigh number and low density ratio, the Reynolds number associated with individual salt fingers may exceed one [8], allowing fingers to drag some fluid around themselves. In order to maintain an overall buoyancy anomaly, the clusters must continuously exchange temperature with the surrounding environment, developing an internal circulation which in a way is reminiscent of the kinematics of a cluster of solid particles [21]. Clusters are then higher-order, doubly diffusive structures, where an effective diffusivity generated by the motion within the cluster plays the role of the temperature diffusivity. This mechanism naturally hints at an upper bound for the scale of the clusters, although in our simulation the scale is bounded by the lateral box size.

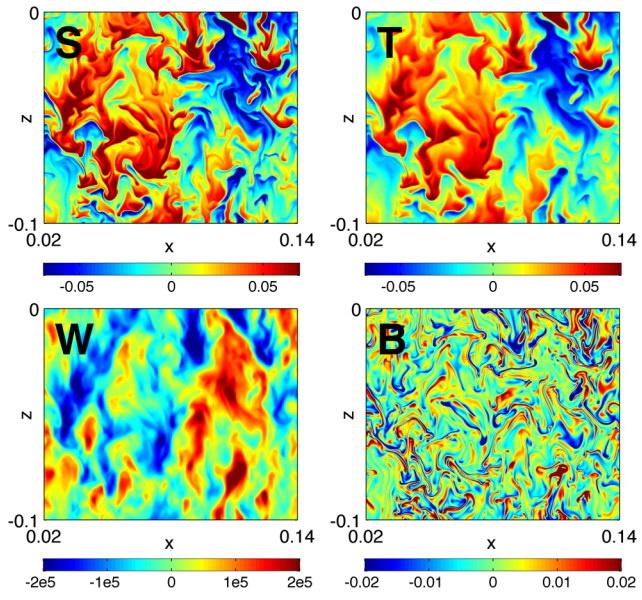

FIG. 3 (color online). Enlargement of a vertical section of the flow at time $t = 3.8 \times 10^{-6}$ and at $y = L_y/2$. The panels show salinity anomaly (upper left), temperature anomaly (upper right), vertical velocity (lower left), and buoyancy anomaly (lower right).

The appearance of the finger clusters is associated also with other large-scale changes in the flow, as demonstrated in Fig. 4, which reports the evolution in time of profiles of horizontally averaged buoyancy, $\bar{B}(z)$, in the central portion of the domain. Starting from an initially vertically constant gradient of buoyancy, the flow develops staircase-like profiles, characterized by the alternation of well-mixed regions with zones with a steep gradient. Similar profiles are found in terms of T and S.

The elusive nature of fingering staircases may be understood by the inability of the individual fingers to stir the background buoyancy gradient. The passage of a finger of size l in a stratified fluid will produce a disturbance of a similar size which is viscously dissipated on a time scale $\tau_\nu \approx l^2/(\text{PrLe})$. In order to stir the stratification, the disturbance must be able to perform a complete roll-up and survive at least for a buoyancy period τ_{buoy} (defined above). The ratio of the two time scales is $\tau_\nu/\tau_{\text{buoy}} \approx \pi/(2\sqrt{\text{Pr}})$ if we use the finger scale l_f defined above, or, alternatively, $\tau_\nu/\tau_{\text{buoy}} \approx \pi/(2\sqrt{\text{Pr}})\sqrt{(R_\rho - 1)/R_\rho}$ if we use the estimate $l_S = \pi[\text{Le}/(R_S R_\rho)]^{0.25}$ due to Stern [5]. In both cases, fingers appear to be ineffective stirrers in a wide parameter range, except at very low Prandtl numbers. A similar argument can be used to show that the disturbances produced by large clusters produce significant stirring in the fluid.

A theoretical analysis [13,14,18] of staircase formation in mechanically stirred, stable stratifications [15,17] suggests that a nonmonotonic dependence of the buoyancy flux on the buoyancy gradient can lead to the formation of staircases. We hypothesize that a similar mechanism is

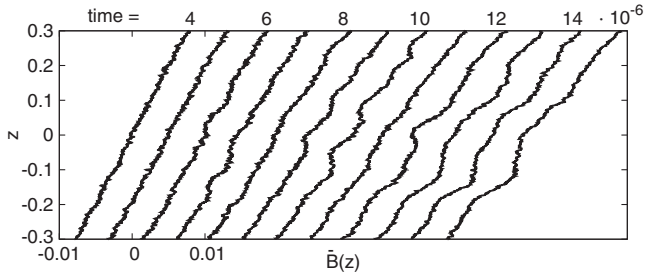

FIG. 4. Time evolution of vertical profiles of horizontally averaged buoyancy, $\bar{B}(x)$, in the central portion of the domain. The frames after the first have been shifted to the right as a function of time.

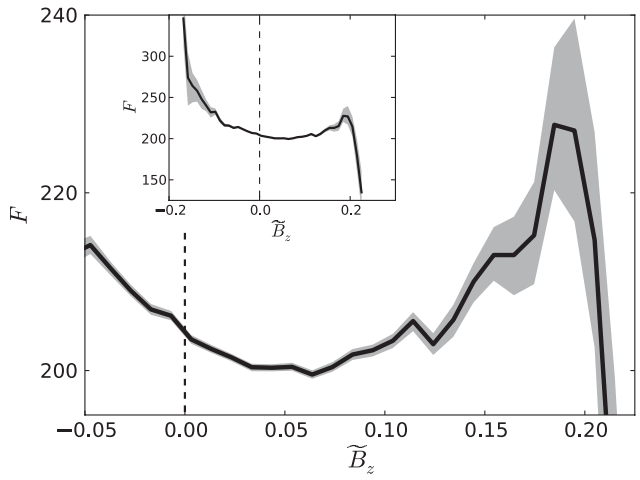

FIG. 5. Average buoyancy flux vs the vertical buoyancy gradient $\tilde{B}_z$. The statistics has been computed from $t = 4 \times 10^{-6}$ to $t = 1.5 \times 10^{-5}$, in the range $-0.3 < z < 0.3$. The gradient has been smoothed by convolution with a Hann window of height $h = 0.01$. The inset shows the complete curve. The grey bands represent 95% confidence bands obtained with a jackknife subsampling procedure.

responsible for staircase formation in fingering convection. From Eqs. (2) and (3), we can derive an equation for the evolution of the average buoyancy profile:

$$\frac{\partial \tilde{B}}{\partial t} + \frac{\partial}{\partial z}\left[\widetilde{wB} - \frac{\partial \tilde{B}}{\partial z} - R_\rho(\mathrm{Le}-1)\frac{\partial \tilde{T}}{\partial z}\right] = 0, \quad (5)$$

where the wavy overbar is both a horizontal average and a vertical convolution with a compactly supported kernel of height h (we use the Hann window). When h is larger than the scale of the fingers, but not larger than the scale of the clusters, then the terms in the squared parenthesis add up to an effective flux F that determines the large-scale evolution of the horizontally averaged, vertically smoothed buoyancy profile $\tilde{B}(z)$. Assuming, as a first approximation, that the flux depends only on the vertical gradient $\tilde{B}_z$, using the chain rule we may rewrite Eq. (5) as

$$\frac{\partial \tilde{B}}{\partial t} = \frac{d(-F)}{d\tilde{B}_z}\frac{\partial^2 \tilde{B}}{\partial z^2}. \quad (6)$$

The local slope of $(-F)$, then, plays the role of an effective diffusion coefficient in a nonlinear diffusion equation for $\tilde{B}$. We report the flux F vs $\tilde{B}_z$ for our simulation in Fig. 5. The curve shows slopes which correspond to a negative diffusion coefficient for intermediate positive values of $\tilde{B}_z$ sandwiched between ordinary diffusion regimes at high and low (or negative) buoyancy gradients. This is compatible with solutions of Eq. (6) alternating regions where $\tilde{B}_z \approx 0$ to regions of high buoyancy gradient and positive effective diffusion such that $F(\tilde{B}_z) \approx F(0)$ [18].

The dominant contribution to F comes from the advective term $\widetilde{wB}$, which is almost two orders of magnitude larger than the other two terms, even where the gradients are the highest. When the stratification is locally top-heavy ($\tilde{B}_z < 0$), both double diffusion and mechanical overturning yield a positive advective flux. For $\tilde{B}_z > 0$, double diffusion gives an up-gradient buoyancy flux ($\widetilde{wB} > 0$) which is opposed by the down-gradient flux produced by the mechanical stirring of the clusters. At low buoyancy gradients, stirring is more effective than double diffusion, and the flux decreases for increasing $\tilde{B}_z$. At larger buoyancy gradients, fast clusters do not have time to exchange temperature with the surrounding fluid quickly enough to maintain their buoyancy anomaly. Therefore, for increasing $\tilde{B}_z$, the clusters slow down or dissolve, losing their stirring ability, while unhampered fingers increase again the net up-gradient flux. The flux cutoff at even larger values of $\tilde{B}_z$ may be understood by observing that very high buoyancy gradients may be attained only in progressively thinner fluid layers, sandwiched between fluid regions with much lower gradients. Since lower local Rayleigh numbers correspond to lower flux [8], as the layers become thinner, the flux diminishes. It is important to notice that if the interval of buoyancy gradients corresponding to positive effective diffusion did not straddle $\tilde{B}_z = 0$, then vertically homogeneous regions with zero buoyancy gradient would not be stable for Eq. (6). Thus, the mechanical mixing of the clusters, which ensures that F decreases across $\tilde{B}_z = 0$, is crucial for staircase formation.

In this Letter, we have presented evidence for a new mechanism of staircase formation in fingering convection, which is neither linked to intrusions [7] nor due to a nonlinear dependence of the flux ratio on the density ratio [10] (in our simulation, the flux ratio is independent of the density ratio). We have verified that the same mechanism operates in two dimensions, in a wide interval of parameters with a set of simulations using a different pseudospectral code, to be reported elsewhere.

[1] J. Turner, Annu. Rev. Fluid Mech. **6**, 37 (1974).
[2] R. Schmitt, Annu. Rev. Fluid Mech. **26**, 255 (1994).
[3] E. Kunze, Progr. Oceanogr. **56**, 399 (2003).
[4] R. Schmitt, J. Ledwell, E. Montgomery, K. Polzin, and J. Toole, Science **308**, 685 (2005).
[5] M. Stern, Tellus **12**, 172 (1960).
[6] P. Baines and A. Gill, J. Fluid Mech. **37**, 289 (1969).
[7] W. Merryfield, J. Phys. Oceanogr. **30**, 1046 (2000).
[8] J. von Hardenberg and F. Paparella, Phys. Lett. A **374**, 2646 (2010).
[9] R. Krishnamurti, J. Fluid Mech. **483**, 287 (2003).
[10] S. Stellmach, A. Traxler, P. Garaud, N. Brummell, and T. Radko, J. Fluid Mech. **677**, 554 (2011).
[11] A. Parodi, J. von Hardenberg, G. Passoni, A. Provenzale, and E. A. Spiegel, Phys. Rev. Lett. **92**, 194503 (2004).
[12] J. von Hardenberg, A. Parodi, G. Passoni, A. Provenzale, and E. Spiegel, Phys. Lett. A **372**, 2223 (2008).

[13] O. Phillips, Deep-Sea Res. Oceanogr. Abstr. **19**, 79 (1972).
[14] E. Posmentier, J. Phys. Oceanogr. **7**, 298 (1977).
[15] S. Thorpe, J. Fluid Mech. **124**, 391 (1982).
[16] B. Ruddick, T. McDougall, and J. Turner, Deep-Sea Res. **36**, 597 (1989).
[17] Y. Park, J. Whitehead, and A. Gnanadeskian, J. Fluid Mech. **279**, 279 (1994).
[18] N. Balmforth, S. Smith, and W. Young, J. Fluid Mech. **355**, 329 (1998).
[19] G. Passoni, G. Alfonsi, and M. Galbiati, Int. J. Numer. Methods Fluids **38**, 1069 (2002).
[20] The MATRIX cluster at CASPUR Supercomputing Center, Rome, Italy, 2011 [http://hpc.caspur.it].
[21] B. Metzger, M. Nicolas, and E. Guazzelli, J. Fluid Mech. **580**, 283 (2007).